Charge compensation and oxidation in $Na_xCoO_{2-\delta}$ and $Li_xCoO_{2-\delta}$ studied by XANES

M. Valkeapää[a],*, Y. Katsumata[a], I. Asako[a], T. Motohashi[a], T.S. Chan[b], R.S. Liu[b],
J.M. Chen[c], H. Yamauchi[a], M. Karppinen[b,d]

[a]*Materials and Structures Laboratory, Tokyo Institute of Technology, Yokohama 226-8503, Japan*
[b]*Department of Chemistry and Center for Nano Storage Research, National Taiwan University, Taipei 10617, Taiwan, Republic of China*
[c]*National Synchrotron Radiation Research Center (NSRRC), Hsinchu 30076, Taiwan, Republic of China*
[d]*Laboratory of Inorganic and Analytical Chemistry, Helsinki University of Technology, FIN-02015 Espoo, Finland*

Abstract

A comparative study on the oxidation and charge compensation in the $A_xCoO_{2-\delta}$ systems, A = Na (x = 0.75, 0.47, 0.36, 0.12) and Li (x = 1, 0.49, 0.05), using X-ray absorption spectroscopy at O 1s and Co 2p edges is reported. Both the O 1s and Co 2p XANES results show that upon removal of alkali metal from $A_xCoO_{2-\delta}$ the valence of cobalt increases more in $Li_xCoO_{2-\delta}$ than in $Na_xCoO_{2-\delta}$. In addition, the data of O 1s XANES indicate that charge compensation by oxygen is more pronounced in $Na_xCoO_{2-\delta}$ than in $Li_xCoO_{2-\delta}$.
© 2007 Published by Elsevier Inc.

1. Introduction

Layered alkali-metal cobalt oxides, $A_xCoO_{2-\delta}$ (A = Na, Li; $0 \leqslant x \leqslant 1$; $0 \leqslant \delta \leqslant \sim 0.3$ [1,2]), have been intensively studied since the 1950s [3–5]. Li_xCoO_2 has attracted attention as an effective cathode material, Na_xCoO_2 as an excellent thermoelectrics, and $Na_xCoO_2 \cdot y\, H_2O$ ($x \approx 0.35$, $y \approx 1.3$) as a superconductor which contains water molecules. After successful preparation of $CoO_{2-\delta}$, i.e. $x = 0$, by electrochemical [6] or chemical [1] deintercalation methods, there has been significant interest in obtaining more information on the electronic structure and properties of the $A_xCoO_{2-\delta}$ system over the whole range of x.

The A^+ cation in $A_xCoO_{2-\delta}$ is located at either trigonal prismatic (P) or octahedral (O) site in between two adjacent CoO_2 layers, consisting of edge sharing CoO_6 octahedra in a hexagonal arrangement. The coordination type, together with the number of CoO_2 layers in the unit cell is used for shorthand classification [4] of the $ACoO_2$ structures. "$P2$" for example denotes a structure in which A^+ is located at a trigonal prismatic site and there are two CoO_2 layers in the unit cell. Two examples of these structure types are shown in Fig. 1. The A^+ cations can reversely enter and leave the O or the P site, retaining the structure intact for the whole x range. Due to this (partial) reversibility, for example, Li_xCoO_2 has been utilized in rechargeable batteries.

If a pure ionic crystal field is assumed, the oxidation state of Co changes from III to IV during charge or upon chemical deintercalation. An ideal deintercalation reaction would be (when using NO_2BF_4 as the oxidant):

$$ACo^{III}O_2 + N^VO_2BF_4 \rightarrow Co^{IV}O_2 + ABF_4 + N^{IV}O_2. \quad (1)$$

However, in A_xCoO_2, like generally in transition-metal (TM) compounds, significant covalency is introduced to the TM–ligand (L = ligand) bonds due to mixing between TM d and L p orbitals. This means that also participation of the ligand in the oxidation process is important. A recent example of this is found in $Ag_2Cu_2O_4$ system, where it has

*Corresponding author. Current Address: Laboratory of Inorganic and Analytical Chemistry, Helsinki University of Technology, FIN-02015 Espoo, Finland. Fax: +358 9 462 373.

E-mail address: markus.valkeapaa@tkk.fi (M. Valkeapää).
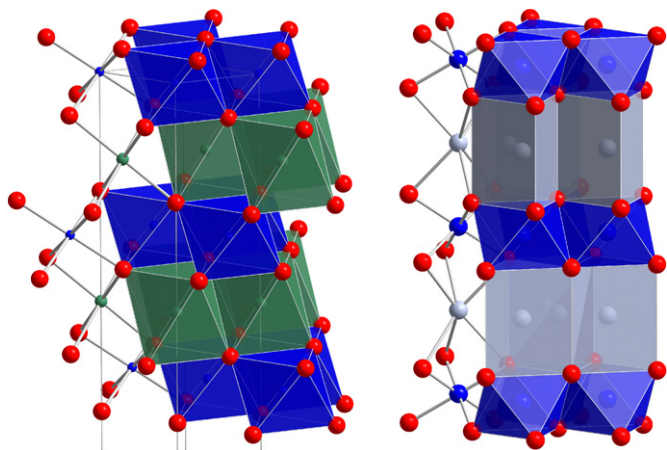
Fig. 1. Examples of different alkali metal coordinations in A_xCoO_2 shown by $O3$ (LiCoO$_2$, left) and $P2$ (Na$_{0.7}$CoO$_2$, right) structure types.

been shown by XPS that oxygen participates in the oxidation process and there is a corresponding increase in the covalency of the TM–O bond [7].

For oxides of Co and other 3d TMs in a crystal field of trigonal D_{3d} (cubic O$_h$) symmetry, mixing takes place mainly between 3d a_{1g} (t_{2g}) levels of TM and 2p levels of oxygen, but TM 4s and 4p orbitals also contribute to the mixing, as observed by, e.g. X-ray absorption spectroscopy [8] (XAS). Thus under strongly oxidative conditions, provided that Co a_{1g} (t_{2g}) and O 2p states are close enough in energy, 2p band will compensate for the lost a_{1g} (t_{2g}) electron (i.e. Co^{III} becomes more electronegative). The resulting redox chemistry of cobalt is not a simple change from Co^{III} to Co^{IV} and vice versa. Instead, electronegativity of Co^{III} increases and at some point the system may become oxygen nonstoichiometric. Similar behavior is well known for chalcogenides [9] and was verified for Li$_x$CoO$_2$, Li$_x$Ni$_{0.85}$Co$_{0.15}$O$_2$, and Li$_x$NiO$_2$ by Chebiam et al. [1,10] by means of oxygen content analysis: Co^{III}, a low spin 3d^6 cation in these materials, has an empty e_g^σ (e_g) band and thus looses an a_{1g} (t_{2g}) electron when oxidized. On the other hand, Ni^{III} of d^7 configuration is oxidized via e_g band. The O 2p band will compensate electron loss for Co^{III} (eventually O^{-II} ions will be oxidized which leads to removal of oxygen from the structure) but not for Ni^{III}. As a result, the cobalt oxidation state stays at ca. $+3.4$ for $x \leqslant 0.5$, but nickel is oxidized to $+3.9$ for $x = 0$ [1]. Besides chemical analysis, it was shown by a Rietveld refinement of synchrotron X-ray powder diffraction data for Li$_x$CoO$_2$ that decreasing x yields oxygen vacancies [11]. Recently it was shown by several techniques [2,12,13] that as x decreases, also Na$_x$CoO$_{2-\delta}$ may become nonstoichiometric. Lower than expected valence values for cobalt have also been observed for Na$_{0.36}$CoO$_{2-\delta}\cdot$1.3 H$_2$O superconductor [12,14].

The so-far accumulated experimental results indicate that oxygen compensates for the electron loss from cobalt upon deintercalation of alkali metal from A_xCoO_2, and that oxidation to Co^{IV} is only partial as x decreases.

According to a polarization-dependent XAS observation by Wu et al. [15], the electronic structure of Na$_x$CoO$_2$ ($x = 0.75$, 0.67, 0.5) exhibits strong Co 3a_{1g}–O 2p characteristics. Similar results were observed for Li$_x$CoO$_2$ films by Yoon et al. [16] who, based on their XAS measurements, reported that charge compensation is achieved in both the O and Co sites simultaneously. On the other hand, Abbate et al. [17] reported, using XAS for bulk LiCo$_{0.9}$Ga$_{0.1}$O$_2$, that there is no oxidation of cobalt to tetravalent state. Apparently there has been no perfect consensus regarding the extend of Co involvement in redox processes, i.e. how much of the Co^{III} cations are actually oxidized to Co^{IV}. It is also interesting to learn to what extend (if any) choice of the alkali metal influences the Co^{III}–Co^{IV} balance. Since XAS probes the unoccupied part of the electronic structure [18] and thus gives information on the electronic states of Co and O in $A_xCoO_{2-\delta}$, it is a useful tool in order to study the aforementioned questions. We collected O 1s and Co 2p X-ray absorption spectra for $A_xCoO_{2-\delta}$ ($A = $ Na, Li) samples, and analyzed them in the X-ray absorption near edge structure (XANES) region as a function of alkali metal content, x ($= 0.75$, 0.47, 0.36, 0.12 for $A = $ Na and 1, 0.49, 0.05 for $A = $ Li).

2. Experimental

Procedures described in previous works [2,19–21] were adapted for the A_xCoO_2 synthesis and subsequent chemical extractions of Li and Na. For the synthesis of Na$_x$CoO$_2$ ($x = 0.75$, 0.70) samples, stoichiometric powder mixtures of Na$_2$CO$_3$ and Co$_3$O$_4$ were placed in a preheated furnace at 800 °C and fired for 12 h [2]. The LiCoO$_2$ sample was prepared by firing a stoichiometric mixture of Li$_2$CO$_3$ and Co$_3$O$_4$ powders for 12 h at 600 °C, being followed by grinding and an additional sintering for 24 h at 900 °C. For the chemical extraction of Na and Li from the synthesized samples, 500 mg portions of Na$_{0.70}$CoO$_2$ and LiCoO$_2$ were treated separately with I$_2$, Br$_2$, and NO$_2$BF$_4$ in CH$_3$CN under stirring. Details of the deintercalation conditions are summarized in Table 1. Reactions with I$_2$ and Br$_2$ were performed in flasks closed in air, whereas all NO$_2$BF$_4$ handling and treatment took place in a glove box filled with Ar. (In addition to NO$_2$BF$_4$, the expected product CoO$_{2-\delta}$ is known to be sensitive to moisture in air, therefore the product was stored and packed in airtight containers inside the glove box.) Also the Br$_2$ treated sample ($A = $ Na) was stored and packed in the Ar filled glove box. Guidelines for handling and storage of the water sensitive samples were adapted from Foo et al. [22].

Resultant cation compositions were determined by inductively coupled plasma optical emission spectroscopy (ICP-OES Prodigy, Leeman Labs). For structural identification and phase purity check, powder X-ray diffraction data with CuK_α radiation were collected (RINT-2500 V diffractometer equipped with a rotating anode, Rigaku). Diffraction patterns were indexed with DICVOL [23] program implemented in the WinPLOTR [24] software

Table 1
Preparation of $A_xCoO_{2-\delta}$ samples by chemical deintercalation of $Na_{0.70}CoO_2$ and $LiCoO_2$, together with the results of ICP-OES analyses

Oxidant	I_2		Br_2		NO_2BF_4	
A	Na	Li	Na	Li	Na	Li
m^a	5	4	75	6	2	2
$V(CH_3CN)$/ml	20	60	20	60	100	60
Time/h	12	65	12	65	12	0.5
Dried in	Glove box	Drying closet	Glove box	Drying closet	Glove box	Vacuum furnace
Drying temperature	Ambient	80 °C	Ambient	80 °C	Ambient	Ambient
x^b	0.47(1)	0.99(4)	0.36(1)	0.49(1)	0.12(1)	0.05(1)

[a] Amount of substance of the used oxidant = $m \times$ theoretical amount of substance needed to remove all A from the compound, cf. reaction (1).

[b] Determined with ICP-OES and normalized to unity in relation to cobalt. As-synthesized samples were also analysed by ICP-OES and their nominal stoichiometry was confirmed.

package. The cell parameters were refined with LeBail [25] method in JANA2000 [26] and FullProf [27] programs.

The XAS measurements were performed on BL20A high-energy spherical grating monochromator beamline at the National Synchrotron Radiation Research Center (NSRRC) in Taiwan. The X-ray photons were monochromatized using horizontal and vertical focusing mirrors, a spherical grating monochromator with 4 gratings, and a toroidal refocusing mirror. The spectra were recorded in X-ray fluorescence-yield (I_f) mode for O 1s absorption, and electron-yield (I_e) mode for Co 2p absorption. The I_f data were collected utilizing a micro channel-plate (MCP) detector system with an electrically isolated grid mounted in front. The grid was set to a voltage of 50 V, the front of the MCPs to −3200 V and the rear to −200 V. The grid bias ensured that positive ions did not enter the detector, while the MCP bias ensured that no electrons were detected. The detector was located at the sample normal, and photons were incident at an angle of 45° with respect to the sample normal. In the I_e mode, the sample drain current was measured. Simultaneously to I_f and I_e, the incident photon flux was monitored by a Ni mesh located after exit slit of the monochromator. All measurements were performed on powder samples at room temperature. The samples of $Na_{0.36}CoO_{2-\delta}$, $Na_{0.12}CoO_{2-\delta}$ and $Li_{0.05}CoO_{2-\delta}$ were unpacked from the containers just before they were loaded in the vacuum chamber. The photon energies were calibrated with an accuracy of 0.1 eV using known absorption peaks of reference compounds. Pre-edge O 1s XANES baselines were set to zero at 526 eV and spectra were normalized to unity at 622 eV, well after the XANES range. In addition, the O 1s spectra were corrected for self-absorption effects by subtracting the calculated absorption of the constituent elements from the spectra. In order to quantify the spectral weights, centroid (= center-of-gravity) abscissa (i.e. energy values) were calculated in WinPLOTR [24].

3. Results

3.1. Chemical and structural characterization

All samples consist of the layered $A_xCoO_{2-\delta}$ structure, and with the exception of $Na_{0.12}CoO_{2-\delta}$ [2] and $Li_{0.05}CoO_{2-\delta}$ which contain two forms of $A_xCoO_{2-\delta}$, are single phased. In Fig. 2, X-ray powder diffraction patterns are shown for the $Li_xCoO_{2-\delta}$ series. The successful deintercalation of A^+ with I_2, Br_2, and NO_2BF_4 is also confirmed by the ICP-OES results shown in Table 1. Note that iodine is not strong enough oxidant for removing Li from $LiCoO_2$. The samples have similar unit cell parameters and the same symmetries as reported in the previous studies [2–5,28–31]. In the $Na_xCoO_{2-\delta}$ series, samples with $x = 0.75$, 0.47, and 0.36 have $P2$ structure in space group $P6_3/mmc$, whereas the $Na_{0.12}CoO_{2-\delta}$ sample is a mixture of $P2$ and $O1$ ($P\bar{3}m1$) [2,5,32] types. $LiCoO_2$ and $Li_{0.99}CoO_2$ have $O3$ [31] structure in space group $R\bar{3}m$, whereas $Li_{0.49}CoO_{2-\delta}$ exhibits a monoclinic unit cell ($O1$) due to Li ordering [6,33,34]. The $Li_{0.05}CoO_{2-\delta}$ sample is a mixture of $P3$ ($R3m$) and $O1$ types. Thus, with the exception of the secondary phase in $Na_{0.12}CoO_{2-\delta}$, oxygen coordination around alkali metal in $Na_xCoO_{2-\delta}$ is prismatic and in $Li_xCoO_{2-\delta}$ octahedral. This means that in each sample series the local structure units stay essentially the same, and consequently, the XANES spectra are not governed by the structural differences but reflect the valence changes in the samples.

The unit cell parameters for the two $A_xCoO_{2-\delta}$ series are plotted in Fig. 3, where the monoclinic cell of $Li_{0.49}CoO_{2-\delta}$ ($P2/m$, $a = 4.86$, 2.81, 5.05 Å, $\beta = 108.65°$) is given as hexagonal for the sake of comparison. The program Truecell implemented in CHEKCELL [35] was used to
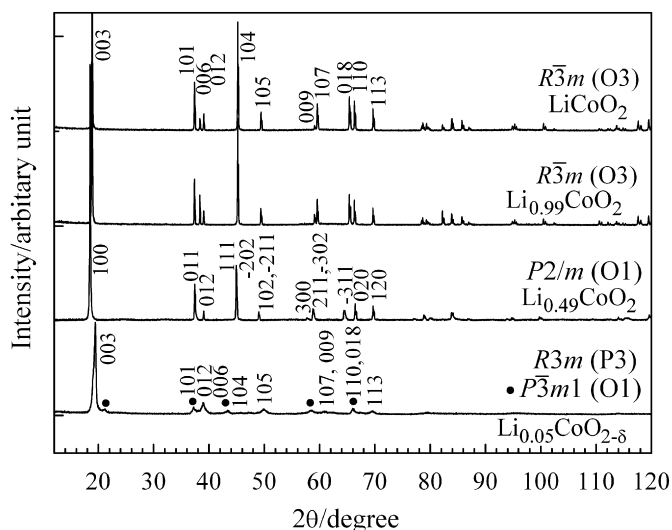
Fig. 2. X-ray powder diffraction patterns together with space groups for $Li_xCoO_{2-\delta}$ samples with different lithium contents. Indices of the main Bragg reflections are given for hexagonal ($LiCoO_2$, $Li_{0.99}CoO_2$ and $P3$ $Li_{0.05}CoO_{2-\delta}$) and monoclinic ($Li_{0.49}CoO_{2-\delta}$) unit cells. $O1$ $Li_{0.05}CoO_{2-\delta}$ phase is marked with ● symbols.
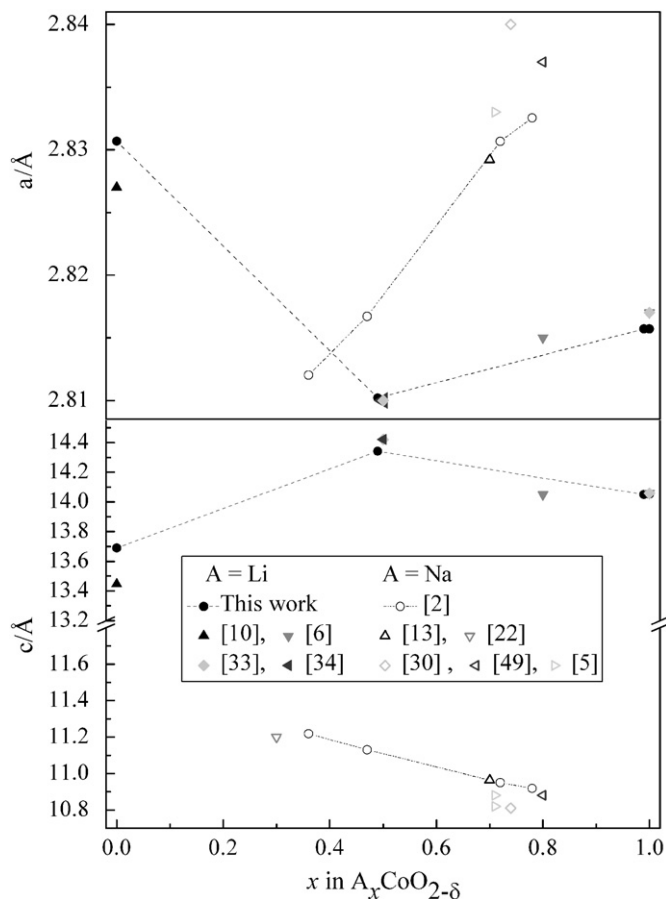
Fig. 3. Unit cell parameters a (upper panel) and c (lower panel) as a function of x for $A_xCoO_{2-\delta}$ samples. Open and closed symbols are for Na- and Li-series, respectively. Monoclinic unit cells of the $x \approx 0.5$ samples have been transformed to hexagonal unit cells.

find the transformation matrix

$$P = \begin{pmatrix} 0 & 1 & 0 \\ -\frac{1}{2} & -\frac{1}{2} & 0 \\ -1 & 0 & -3 \end{pmatrix}$$

for the conversion $(\mathbf{a}_{mono}, \mathbf{b}_{mono}, \mathbf{c}_{mono}) = (\mathbf{a}_{hexa}, \mathbf{b}_{hexa}, \mathbf{c}_{hexa})\mathbf{P}$.

For the $Na_xCoO_{2-\delta}$ samples the alkali metal removal results in a decrease in a and an increase in c. These changes can be attributed to an increase in the Co valence and/or in the number of O vacancies (affecting a) and the stronger electrostatic repulsion between CoO_2 layers (affecting c). A similar trend is seen in the $Li_xCoO_{2-\delta}$ series until $x \approx 0.5$, but for $x < 0.5$ the reverse is observed: a increases and c decreases as Li is removed from $Li_{0.49}CoO_{2-\delta}$.

3.2. O 1s XANES

To a very close approximation, O 1s X-ray absorption spectrum repeats the oxygen p-projected DOS and the spectrum has no influence from the core hole, as is shown by comparisons between the calculated ground state DOS

and the experimental spectra [36]. Oxygen and other ligand 1s XANES are thus treated as if they resulted from single particle processes and the spectral features are assigned accordingly.

Figs. 4 and 5 show O 1s absorption spectra for $Na_xCoO_{2-\delta}$ and $Li_xCoO_{2-\delta}$ samples, respectively. The two main features seen in Figs. 4a and 5a are common for each spectrum: ∼5 eV broad pre-edge region about 530 eV and a wider region between ∼534 ("rising edge") and ∼548 eV. These correspond to transitions from O 1s core levels to O 2p–Co 3d and to O 2p–Co 4sp mixed states and are general features for transition metal oxides with octahedrally coordinated metal, as shown by de Groot et al. [8]. Moreover, these features are not restricted to any particular array of octahedra in the layer since they are present in spectra from other types of oxides as well (e.g. $La_{1-x}Sr CoO_{3-\delta}$ [37–39] and $La_{2-x}Sr_xLi_{0.5}Co_{0.5}O_4$ [38,40]), and are very similar for O_h and D_{3d} coordination symmetries. Other XANES studies on $A_xCoO_{2-\delta}$ and on
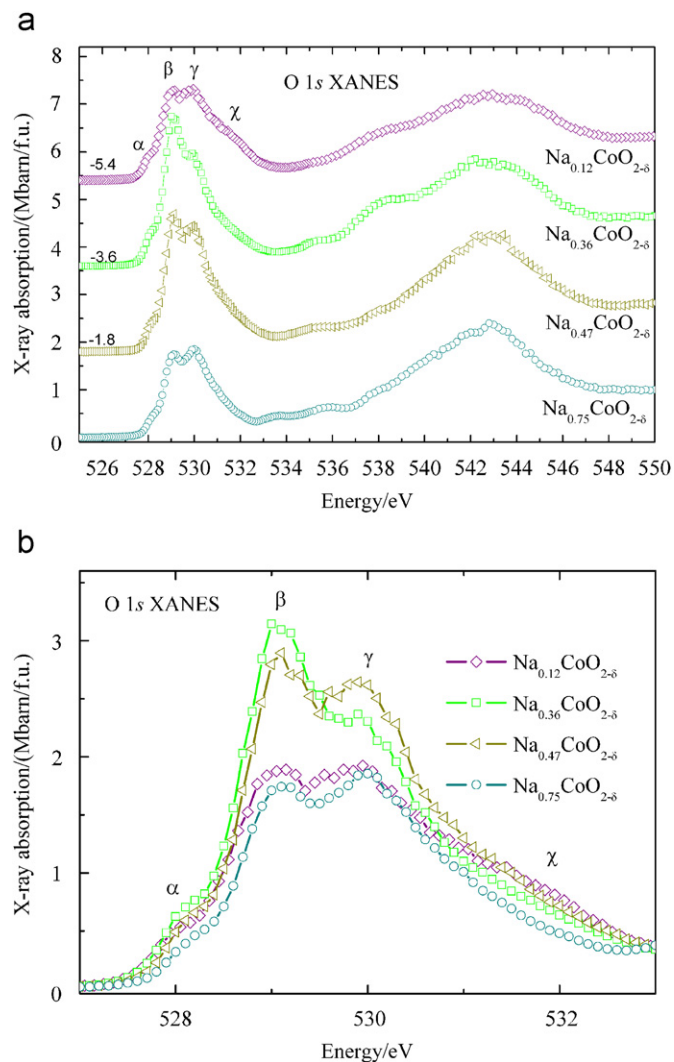
Fig. 4. O 1s XANES spectra of (a) $Na_xCoO_{2-\delta}$ and (b) magnified view from the pre-edge region of the same spectra. Assignment of pre-edge features α, β, γ, and χ to different electronic states is explained in the text.

a

b
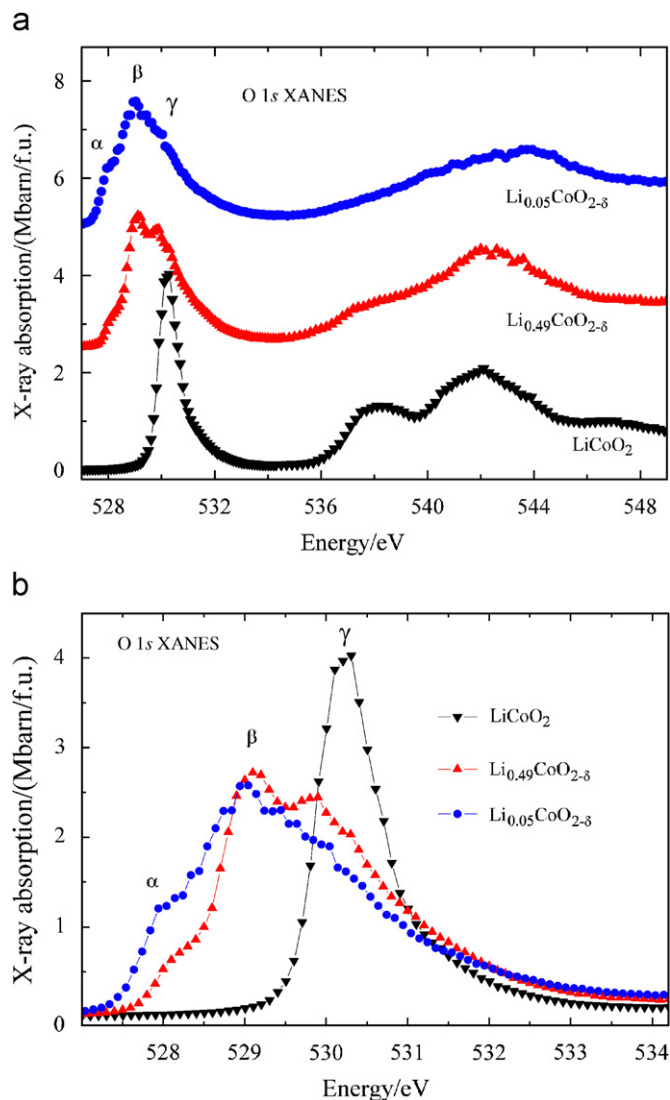
Fig. 5. O 1s XANES spectra of (a) $Li_xCoO_{2-\delta}$ and (b) magnified view from the pre-edge region of the same spectra.

related misfit layered cobalt oxides also show the same features [15,16,41–43].

Assignment of spectral features α, β, and γ on specific electronic structures in the O 2p–Co 3d system arises naturally from considering the $LiCoO_2$ spectra, since $LiCoO_2$ is a well-known host for low spin Co^{III}. The sharp and single peak γ for $LiCoO_2$ at ∼530 eV in Fig. 5a originates from transitions to unoccupied O 2p–Co 3d e_g^σ hybridized states. The changes in the electronic structure of Co upon decreasing x are seen on the lower energy side of γ. Peaks α at ∼528 eV and β at ∼529 eV are assigned for transitions to O 2p states which are hybridized with a_{1g} and e_g^σ states of Co^{IV}, respectively. The use of a_{1g} assumes distorted CoO_6 octahedra of D_{3d} symmetry which is the case for CoO_2 layers in $A_xCoO_{2-\delta}$. A corresponding assignment, in terms of relative energy levels, can be made by assuming O_h symmetry and replacing a_{1g} with t_{2g}. We employ D_{3d} since in addition to the crystallographic reasoning, the results of polarization dependent XANES

performed on $Na_{0.5}CoO_{2-\delta}$ single crystals [42] strongly support it. An example of assignment for the O_h crystal field is given elsewhere [40].

Upon the removal of alkali metal, α and β appear already at $x = 0.75$ and increase in relation to γ as the alkali metal content further decreases. For $Na_{0.12}CoO_{2-\delta}$, however, β and γ have the same intensities. In addition to increasing spectral weight on the lower energy side, some broadening of the tail of γ towards the higher energy (χ) takes place upon decreasing x in the $Na_xCoO_{2-\delta}$ series, as seen in the magnified pre-edge region of Fig. 4b. Since this broadening takes place at higher energy than γ, it is assigned to an increased number of O 2p holes. In the $Li_xCoO_{2-\delta}$ spectra, such broadening is less significant (Fig. 5b). It is also seen that there is a small shift of α and β towards lower energy for $Li_xCoO_{2-\delta}$ as x decreases but not for $Na_xCoO_{2-\delta}$. The energy difference between $LiCoO_2$ and $Li_{0.05}CoO_{2-\delta}$ O 1s pre-edge is 2.1 eV, in agreement with a change in the formal valence of cobalt from III to IV (compare with, e.g. a shift of 2.3 eV between Fe^{II} and Fe^{III} in Ref. [44] or ∼2 eV between Co^{III} and Co^{IV} in Ref. [16]), whereas the largest difference in the Na-series is ∼0.4 eV, indicating only small changes in the cobalt (and oxygen) valence. Pre-edge regions for the both series are shown in Fig. 6. In order to numerically evaluate the changes in the spectral weight, plot of O 1s pre-edge peak centroid energy vs. alkali metal content for $Na_xCoO_{2-\delta}$ and $Li_xCoO_{2-\delta}$ samples is shown in Fig. 7. The centroid energy for $Na_xCoO_{2-\delta}$ samples remains almost constant for all values of x, whereas there is a clear shift for the $Li_xCoO_{2-\delta}$ samples. Thus, based on both the pre-edge (onset) position and the spectral weight, O 1s XANES indicates that valance of cobalt increases in $Li_xCoO_{2-\delta}$ but not significantly in $Na_xCoO_{2-\delta}$ samples, as x decreases. Moreover, in the case of $Li_xCoO_{2-\delta}$, there is a small decrease in
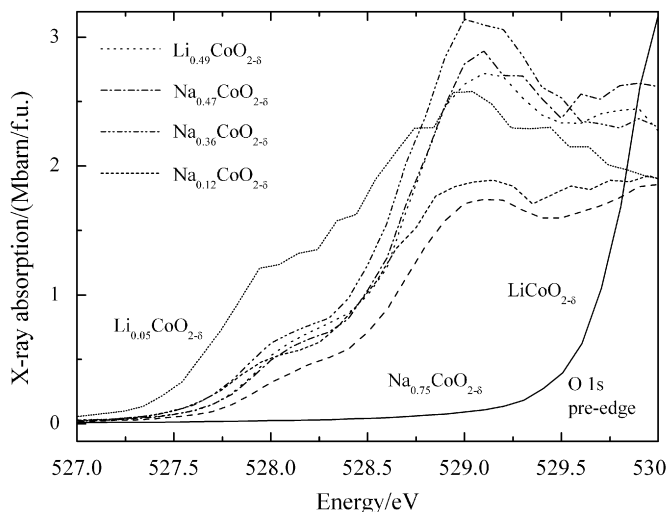
Fig. 6. A detail of the O 1s XANES pre-edge region for the $A_xCoO_{2-\delta}$ (A = Na, Li) series. The apparent shift towards lower energy, as x decreases, indicates increased oxidation of cobalt.
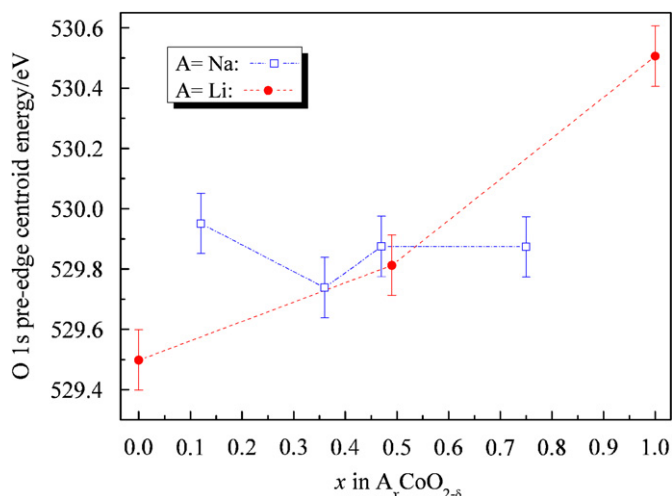
Fig. 7. O 1s XANES pre-edge energy vs. x in $A_xCoO_{2-\delta}$ using (a) centroid and (b) first derivative to determine the positions.

the slope below $x = 0.49$ which indicates less increase in V(Co).

3.3. Co 2p XANES

According to the selection rules for allowed transitions, 2p X-ray absorption spectrum probes both $2p^63d^n \rightarrow 2p^5p^{\square}3d^{n+1}$ and $2p^5p^{\square}4s^n \rightarrow 2p^54s^{n+1}$ transitions but is in practice strongly dominated by the first. Unlike the 1s XANES, where the core hole has no significant effect on the spectrum, 2p XANES is affected by the multiplet effects (i.e. overlap between the core and 3d wave functions [36]), which split or broaden the absorption edge spectrum.

Since the energies of $2p_{3/2}$ ($\sim$778 eV) and $2p_{1/2}$ ($\sim$792 eV) edges are close to each other and the branching ratio $BR = I(2p_{3/2})/I(2p_{3/2}) + I(2p_{1/2})$ of their relative intensities can give information on the spin state of the TM, both are usually covered in the TM 2p XAS experiment. Co 2p XAS branching ratio values for LS and HS configurations should be $\sim$0.6 and $\sim$0.7, respectively [38,45]. As was mentioned earlier, Co^{III} is expected to have a LS configuration in $LiCoO_2$. This is supported by BR value of 0.63. Since BR for all the other spectra is 0.63–0.64 we conclude that Co has LS configuration in all of our samples. Also the shapes of spectra suggest LS configuration since, according to calculated spectra, the shoulders at $\sim$780 and $\sim$794 eV would be missing in the case of HS cobalt [15].

Fig. 8 shows Co $2p_{3/2}$ and $2p_{1/2}$ (insert) absorption spectra for $Na_xCoO_{2-\delta}$ and $Li_xCoO_{2-\delta}$ samples, together with a reference spectrum collected from Co_3O_4. The shoulders seen for the $2p_{3/2}$ and $2p_{1/2}$ peaks show the presence of multiplet effects which can be successfully analyzed by multiplet theory [46], even if such analysis is not presented here. For the Li-series, a shift of ca. $+0.5$ eV together with a decrease in intensity is seen between the spectra of $LiCoO_2$ and $Li_{0.05}CoO_{2-\delta}$, indicating an increase of cobalt valence as x decreases. In electrochemically
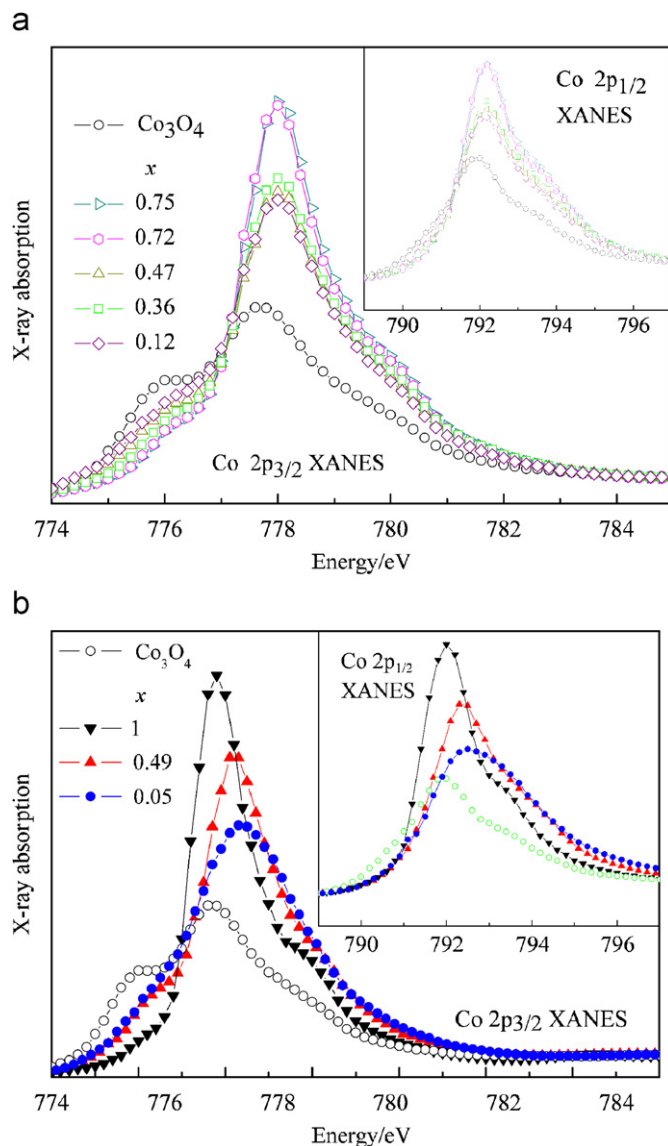
Fig. 8. Co $2p_{3/2}$ and $2p_{1/2}$ (insert) XANES spectra of (a) $Na_xCoO_{2-\delta}$ and (b) $Li_xCoO_{2-\delta}$.

deintercalated thin film samples of $Li_xCoO_{2-\delta}$ ($1 \leqslant x \leqslant 0.25$) corresponding shifts were found to be $+0.7$ and $+0.8$ eV, respectively [16]. Positive shifts in TM 2p XANES peak positions due to the increased formal valence of the TM are observed for other TM compounds as well [16,38,47,48]. For the Na-series Co $2p_{1/2}$ and $2p_{3/2}$ absorption edge energies stay the same for all the samples but there is a decrease in the intensity between the samples of high ($x = 0.75$) and low ($x = 0.47, 0.36, 0.12$) alkali metal contents. Plots of centroid energy vs. alkali metal content for $Na_xCoO_{2-\delta}$ and $Li_xCoO_{2-\delta}$ samples are shown in Fig. 9. In the case of Co $2p_{1/2}$ edge (upper part) the plot agrees very well with the above discussion on peak positions. The data points from the Co $2p_{3/2}$-edge, although more spread, do also show increasing separation between the centroid energies for $A = Na$ and $A = Li$ series, as x decreases. Moreover, in the case of $A = Li$, there is a small decrease in the slope below $x = 0.49$, which
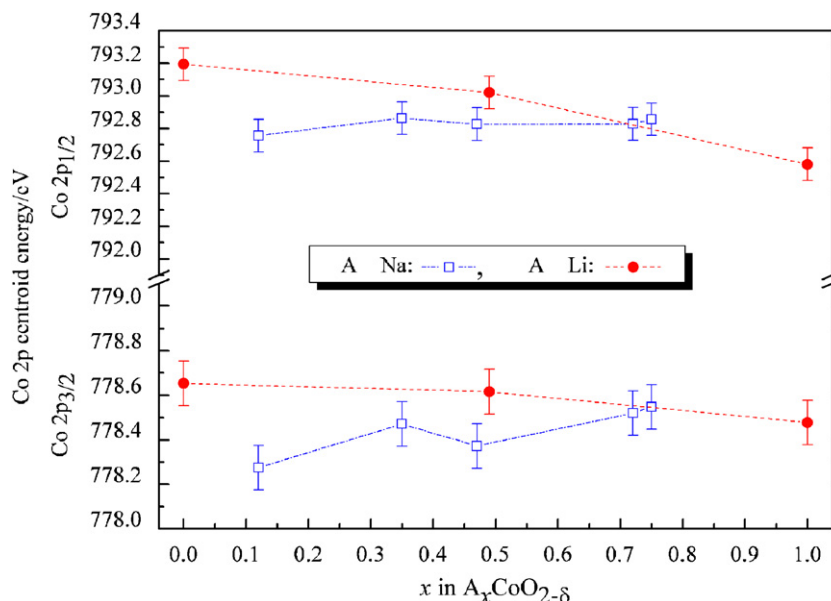
Fig. 9. Co 2p XANES peak position (centroid's abscissa) vs. x in $A_x CoO_{2-\delta}$.

indicates less increase for V(Co). Thus, like the O 1s XANES, Co 2p XANES results also indicate that upon decreasing x, cobalt valence continues to increase in the Li-series but not in the Na-series.

4. Discussion

Inspection of the peak positions and centroid energies indicates that as x decreases, cobalt valence seems to increase in $Li_x CoO_{2-\delta}$ but not in $Na_x CoO_{2-\delta}$. However, keeping in mind that not only absorption energy but also peak intensity is sensitive to the changes in the ligand-metal covalency [44] attention is given to the integrated intensity (Gaussian fit) of the spectra (Fig. 10). It is seen that for both series x has a threshold point, below which the oxidation does not continue for the Na-series or continues to a lesser extend for the Li-series. The x value for this point is similar in both series: ~0.5 in $Li_x CoO_{2-\delta}$ and ~0.4 in $Na_x CoO_2$ and in accordance with the results of wet-chemical analyses [1,2,10,12]. Another intensity related feature is the broadening at ~531 eV (χ in Fig. 4b) which is present for the Na-series but not for the Li-series. The χ feature suggests that upon deintercalation the number of O 2p holes increases more in $Na_x CoO_{2-\delta}$ than in $Li_x CoO_{2-\delta}$. This would mean that oxygen bound to sodium has more electron density available for charge compensation to cobalt, as also expected from the electronegativities of Li and Na.

5. Conclusion

We measured X-ray absorption spectra of several $A_x CoO_{2-\delta}$ samples and studied them in the XANES region as a function of alkali metal content, x (= 0.75, 0.47, 0.36, and 0.12 for A = Na; 1, 0.49, and 0.05 for A = Li).
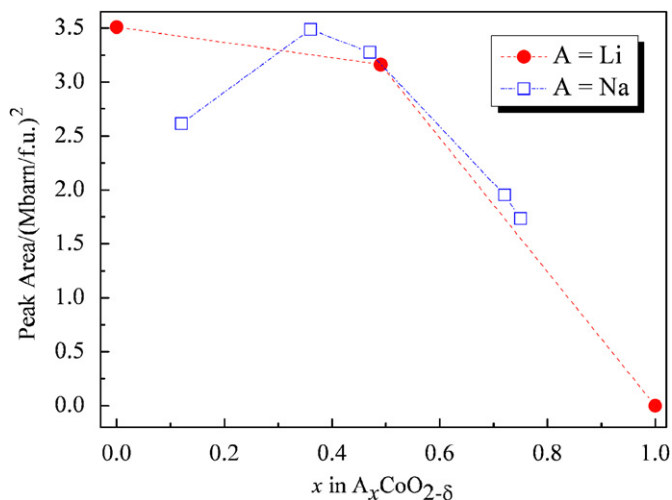
Fig. 10. Integrated O 1s pre-edge intensity vs. x for $A_x CoO_{2-\cong}$ samples.

According to the Co 2p XAS branching ratio, Co has the low spin configuration in all samples. Our XANES experiments show that as x decreases, cobalt valence increases more in $Li_x CoO_{2-\delta}$ than in $Na_x CoO_{2-\delta}$ and that the alkali metal content x has a threshold point, below which the oxidation does not continue for the Na-series or continues to a lesser extend for the Li-series. The x value for this point is ~0.5 in $Li_x CoO_{2-\delta}$ and ~0.4 in $Na_x CoO_{2-\delta}$.

References

[1] R.V. Chebiam, F. Prado, A. Manthiram, Chem. Mater. 13 (2001) 2951–2957.

[2] M. Karppinen, I. Asako, T. Motohashi, H. Yamauchi, Phys. Rev. B 71 (2005) 092104–092105.

[3] C. Delmas, J.-J. Braconnier, C. Fouassier, P. Hagenmuller, Solid State Ionics 3-4 (1981) 165.

[4] C. Delmas, C. Fouassier, P. Hagenmuller, Physica B 99 (1980) 81–85.

[5] C. Fouassier, G. Matejka, J.-M. Reau, P. Hagenmuller, J. Solid State Chem. 6 (1973) 532–537.

[6] G.G. Amatucci, J.M. Tarascon, L.C. Klein, J. Electrochem. Soc. 143 (1996) 1114–1123.

[7] D. Munoz-Rojas, G. Subias, J. Fraxedas, P. Gomez-Romero, N. Casan-Pastor, J. Phys. Chem. B 109 (2005) 6193–6203.

[8] F.M.F. de Groot, M. Grioni, C. Fuggle, J. Ghijsen, G.A. Sawatsky, H. Petersen, Physica B 40 (1989) 5715–5723.

[9] J. Rouxel, Curr. Sci. 73 (1997) 31–39.

[10] R.V. Chebiam, F. Prado, A. Manthiram, J. Solid State Chem. 163 (2002) 5–9.

[11] J.M. Tarascon, G. Vaughan, Y. Chabre, L. Seguin, M. Anne, P. Strobel, G. Amatucci, J. Solid State Chem. 147 (1999) 410–420.

[12] M. Karppinen, I. Asako, T. Motohashi, H. Yamauchi, Chem. Mater. 16 (2004) 1693–1696.

[13] K. Takada, M. Osada, F. Izumi, H. Sakurai, E. Takayama-Muromachi, T. Sasaki, Chem. Mater. 17 (2005) 2034–2040.

[14] P.W. Barnes, M. Avdeev, J.D. Jorgensen, D.G. Hinks, H. Claus, S. Short, Phys. Rev. B 72 (2005) 134515–1345158.

[15] W.B. Wu, D.J. Huang, J. Okamoto, A. Tanaka, H.J. Lin, F.C. Chou, A. Fujimori, C.T. Chen, Phys. Rev. Lett. 94 (2005) 146402–146404.

[16] W.S. Yoon, K.B. Kim, M.G. Kim, M.K. Lee, H.J. Shin, J.M. Lee, J.S. Lee, C.H. Yo, J. Phys. Chem. B 106 (2002) 2526–2532.

[17] M. Abbate, S.M. Lala, L.A. Montoro, J.M. Rosolen, Phys. Rev. B 70 (2004) 235101–235104.

[18] J.C. Fuggle, I.J.E. Unoccupied, Electronic States, Springer, Berlin, 1992.

[19] T. Motohashi, E. Naujalis, R. Ueda, K. Isawa, M. Karppinen, H. Yamauchi, Appl. Phys. Lett. 79 (2001) 1480–1482.

[20] S. Venkatraman, A. Manthiram, Chem. Mater. 14 (2002) 3907–3912.

[21] A.R. Wizansky, P.E. Rauch, F.J. Disalvo, J. Solid State Chem. 81 (1989) 203–207.

[22] M.L. Foo, T. Klimczuk, R.J. Cava, Mat. Res. Bull. 40 (2005) 665–670.

[23] A. Boultif, D. Louër, J. Appl. Cryst. 37 (2004) 724–731.

[24] T. Roisnel, J. Rodríguez-Carvajal, in: Proceedings of the Seventh European Powder Diffraction Conference, 2000, pp. 118–123.

[25] A. Le Bail, Abstracts of the Satellite Meeting on Powder Diffraction of the XV Congress of the IUCr, 1990, p. 99.

[26] V. Petricek, M. Dusek, The Crystallographic Computing System JANA2000, Institute of Physics, Praha, Czech Republic, 2000.

[27] J. Rodríguez-Carvajal, Abstracts of the Satellite Meeting on Powder Diffraction of the XV Congress of the IUCr, 1990, p. 127.

[28] K. Mizushima, P.C. Jones, P.J. Wiseman, J.B. Goodenough, Mat. Res. Bull. 15 (1980) 783–789.

[29] I. Terasaki, Y. Sasago, K. Uchinokura, Phys. Rev. B 56 (1997) 12685–12687.

[30] R.J. Balsys, R. Lindsay, Davis Solid State Ionics 93 (1996) 279–282.

[31] H.J. Orman, P.J. Wiseman, Acta Cryst. C 40 (1984) 12–14.

[32] Y. Takahashi, Y. Gotoh, J. Akimoto, J. Solid State Chem. 172 (2003) 22–26.

[33] J.N. Reimers, J.R. Dahn, J. Electrochem. Soc. 139 (1992) 2091–2097.

[34] Y. Shao-Horn, S. Levasseur, F. Weill, C. Delmas, J. Electrochem. Soc. 150 (2003) A366–A373.

[35] J. Laugier, B. Bochu, CHEKCELL: Powder Indexing Helper Tool for Unit Cell and Spacegroup Assignment, Laboratoire des Matériaux et du Génie Physique (LMGP), France, version 11.01.2004.

[36] F.M.F. De Groot, Chem. Rev. 101 (2001) 1779–1808.

[37] M. Abbate, C.J. Fuggle, A. Fujimori, L.H. Tjeng, C.J. Chen, R. Potze, G.A. Sawatsky, H. Eisaki, S. Uchida, Phys. Rev. B 47 (1993) 16124–16130.

[38] Z. Hu, C. Grazioli, M. Knupfer, M.S. Golden, J. Fink, P. Mahadevan, A. Kumar, S. Ray, D.D. Sarma, S.A. Warda, J. Alloys Compd. 343 (2002) 5–13.

[39] O. Toulemonde, N. N'Guyen, F. Studer, A. Traverse, J. Solid State Chem. 158 (2001) 208–217.

[40] S.A. Warda, W. Massa, D. Reinen, Z. Hu, G. Kaindl, F.M.F. de Groot, J. Solid State Chem. 146 (1999) 79–87.

[41] M. Kubota, K. Takada, T. Sasaki, H. Kumigashira, J. Okabayashi, M. Oshima, M. Suzuki, N. Kawamura, M. Takagaki, K. Fukuda, K. Ono, Phys. Rev. B 70 (2004) 012508–012511.

[42] T. Mizokawa, L.H. Tjeng, H.J. Lin, C.T. Chen, R. Kitawaki, I. Terasaki, S. Lambert, C. Michel, Phys. Rev. B 71 (2005) 1931071–1931074.

[43] T. Mizokawa, L.H. Tjeng, P.G. Steeneken, N.B. Brookes, I. Tsukada, T. Yamamoto, K. Uchinokura, Phys. Rev. B 64 (2001) 1151010–1151041.

[44] T. Glaser, B. Hedman, K.O. Hodgson, I. Edwards, E.I. Solomon, Acc. Chem. Res. 33 (2000) 859–868.

[45] B.T. Thole, D. van der Laan, Phys. Rev. B 38 (1988) 3158–3171.

[46] F.M.F. de Groot, Coordin. Chem. Rev. 249 (2005) 31–63.

[47] Z. Hu, G. Kaindl, S.A. Warda, D. Reinen, F.M.F. de Groot, B.G. Muller, Chem. Phys. 232 (1998) 63–74.

[48] Z. Hu, M.S. Golden, J. Fink, G. Kaindl, S.A. Warda, D. Reinen, P. Mahadevan, D.D. Sarma, Phys. Rev. B 61 (2000) 3739–3744.